Journal of Japan Association for Earthquake Engineering, Vol. 19, No. 8, 2019

INVESTIGATION OF NATURAL FREQUENCY REDUCTION MECHANISM OF A HISTORIC MASONRY BUILDING IN PATAN FOLLOWING THE 2015 GORKHA EARTHQUAKE IN NEPAL

Aiko FURUKAWA[1], Rikuto HANAFUSA[2], Junji KIYONO[3] and Rishi R. PARAJULI[4]

[1] Member of JAEE, Associate Professor, Department of Urban Management, Kyoto University, Kyoto, Japan, furukawa.aiko.3w@kyoto-u.ac.jp
[2] Master Course Student, Department of Urban Management, Kyoto University, Kyoto, Japan
[3] Member of JAEE, Professor, Department of Urban Management, Kyoto University, Kyoto, Japan, kiyono.junji.5x@kyoto-u.ac.jp
[4] Lecturer, Institute of Engineering, Tribhuvan University, Kathmandu, Nepal

ABSTRACT: On April 25, 2015, Gorkha earthquake occurred about 80 km northwest of Kathmandu. In Patan, masonry structures collapsed in Durbar Square. The two-story masonry building that is the subject of this study, is about a 5-minute walk from Durbar Square. Although the building did not collapse, cracks were confirmed in several places. Microtremor measurements performed before and after the earthquake revealed that the natural frequencies of the building decreased. This study examined the factors that decrease the natural frequencies of buildings by seismic response analysis using ground motion estimated by the H/V spectrum ratio as input.

Key Words: Nepal, Historic masonry building, Gorkha earthquake, Damage analysis, Refined DEM

1. INTRODUCTION

With its three major former royal cities, i.e., Kathmandu, Patan and Bhaktapur, Kathmandu Valley is a center of culture in Nepal. Unfortunately, a large number of historic buildings have been damaged due to earthquakes over the centuries as it is located on the earthquake-prone zone of the Himalayan orogen[1), 2)].

Kathmandu Valley was registered in a list of endangered Cultural Heritage sites in 2003 because numerous buildings of cultural heritage in this region were demolished in the process of industrialization and commercialization. As a result of the efforts of the World Heritage Committee and associated ministries of Nepal, the valley was removed from the endangered list in 2007[3)]. However, despite the many efforts to protect the cultural heritage, the protection of buildings from earthquake disasters is insufficient.

Since a mega-earthquake is predicted to occur at the Himalayan orogen in the west of Kathmandu[4),5),6)], and it has been pointed out that the surface ground in Kathmandu is very soft and

amplifies ground motion largely[7),8)], it is important to take countermeasures against earthquakes. Nepal has a major tourist industry and earthquake damage to its cultural heritage would negatively affect the country's economy. Protecting the tourist resources that support the lives of many people is important, as is securing Nepal's cultural heritage for future generations.

The Japanese government has been providing technical assistance through JICA. In 2002, seismic damage to buildings in Kathmandu was estimated by a simple method utilizing a structural vulnerability function[9)]. However, since the used vulnerability function is statistically constructed from past earthquake data worldwide, it is not necessarily suitable for Kathmandu.

We assessed the seismic safety of a two-story historic masonry building (target building) located a 5-minute walk from Patan Durbar Square[10)] from 2008 to 2012 as part of the Ritsumeikan University Global COE Program (Global COE for Education, Research and Development of Strategy on Disaster Mitigation of Cultural Heritage and Historic Cities). Microtremor observations of the target building were conducted and natural frequencies were obtained. A numerical model of the refined distinct element method (refined DEM) was created based on the material properties obtained by static loading test, and the validity of the numerical model was confirmed by comparing the analytical and the measured natural frequencies of the first mode. Earthquake response analysis of the model was then conducted by inputting ground motions obtained by probabilistic seismic hazard analysis. The DEM analysis results indicated that the building would suffer partial damage without collapsing for an earthquake level with a return period of 98 years, but total building collapse was predicted for earthquake levels with return periods of both 475 and 975 years[10)].

The M_w 7.8 Gorkha earthquake struck the region of Kathmandu on April 25, 2015. We visited the building site again and investigated the building damage. The target building survived the earthquake, and it was difficult to find new cracks by a visual inspection from outside the building. However, microtremor observations revealed that the natural frequencies of the building after the earthquake were decreased compared to those before the earthquake[11)]. The post-earthquake visual inspection inside the building revealed several new cracks[11)]. This paper presents our investigation of the causes of the natural frequency reduction of the target building.

The structure of this paper is as follows. Chapter 2 describes the damage situation and observed natural frequencies. Chapter 3 presents a numerical model that can express the first five natural frequencies of the pre-earthquake condition with good accuracy. Chapter 4 describes the microtremor observation results of the surface ground at the building site and the earthquake observation sites. Since the vibration characteristics of the surface ground at the building site were different from those at the earthquake observation sites, the ground acceleration at the building site was estimated by an empirical method using the H/V spectral ratio. In Chapter 5, the earthquake response analysis of the numerical model established in Chapter 3 and the ground acceleration estimated in Chapter 4 as input was conducted. When we applied the tensile strength values stated in the Indian building code[12)] used in Nepal, more cracks were judged to be generated and the natural frequencies became lower by the numerical analysis compared to the actual situation observed during the post-earthquake damage survey. This revealed the possibility that the actual tensile strength of the target building was larger than the value shown in the building code. In numerical analysis using a numerical model that allows for damage at locations where actual damage is observed, the reduction of the natural frequency was explained with good accuracy.

2. TARGET BUILDING

2.1 Target building and crack occurrence situation

The target building is a historic masonry building consisting of bricks and timber as shown in Fig. 1. It is used for public purposes by nearby residents and considered as a temporary shelter in the case of earthquakes. It was built in the seventeenth century, but it has been repaired many times due to damage caused by earthquakes and aging. The building is two-storied and has dimensions of 16.5 m × 5.6 m.

The height of the 1st and 2nd floors is 2.4 m and 2.2 m, respectively. The maximum height is 6.5 m. Each wall has openings, and the western wall has the largest openings. The walls are composed of bricks and mortar. There are two separate narrow rooms as shown in Fig. 2.

(a) Before earthquake (November 3, 2009)

(b) After earthquake (March 5, 2016)

Fig. 1 Appearance of building before and after the 2015 Gorkha earthquake
(Left: South side, Middle: East side, Right: West side)

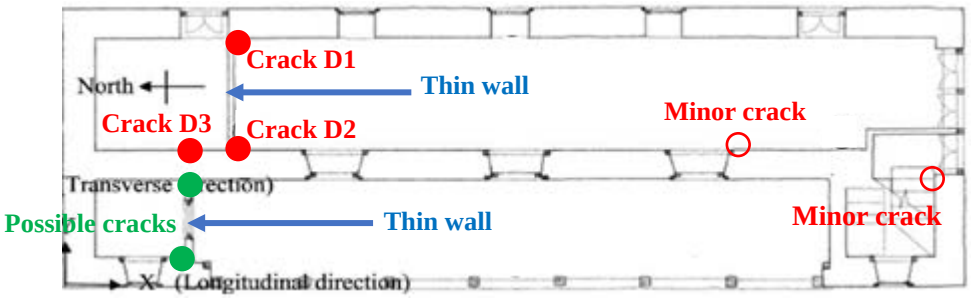

(a) Location of cracks on the 1st floor

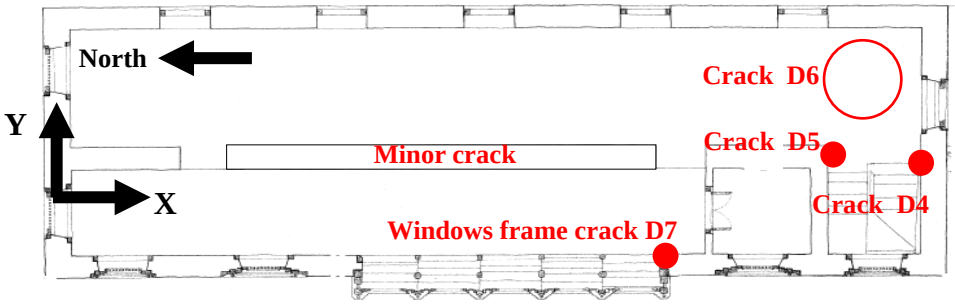

(b) Location of cracks on the 2st floor

Fig. 2 Location of cracks found in the building after the 2015 Gorkha earthquake
(The left is the north and the top is the east.)

Figure 1(a) and (b) respectively show the appearance of the building from the outside before and after the earthquake. It was difficult to find new cracks from outside the building. Figure 2 shows the locations where cracks were found inside the building by visual inspection after the earthquake. The left is the north and the top is the east. Since no comparable photographs were taken prior to the earthquake, it is difficult to judge whether the cracks found inside the buildings existed before the earthquake or were generated due to the earthquake, but those cracks appeared to be new. For example, the photograph of cracks found at D1 is shown in Fig. 3(a). A similar crack was found at D2. We considered that the cracks were generated at D1 and D2 due to the earthquake since the thin wall between D1 and D2 resisted the out-of-plane deformation of the longitudinal wall. We also found cracks at the boundary between the thin wall and the ceiling. In the same manner, the building has a thin wall (the wall between green circles ●) in the western part of the first floor (the lower part of Fig. 2(a)). Unfortunately, we were not allowed to enter the western part of the first floor, and the visual inspection could not be conducted in this part. But we assume that cracks similar to D1 and D2 were generated at the intersection part shown by green circles ● since we found a crack at D3 as shown in Fig. 3(b) in the small room in the north-eastern corner of the first floor.

2.2 Acceleration record

The locations of the epicenter of Gorkha earthquake and the target building in Patan are shown in Fig. 4(a) [13]. The distance between the epicenter and the building is about 78 km. Figure 4(b) is a map showing the locations of the target building and the observation sites. Station KATNP is a United States Geological Survey (USGS) strong-motion station[14]. Acceleration was also observed at four observation stations, KTP, TVU, PTN installed by Takai et al. [15]. The nearest station to the target building is PTN.

(a) Crack at D1 (b) Crack at D3

Fig. 3 Photographs of cracks found in the building after the 2015 Gorkha earthquake

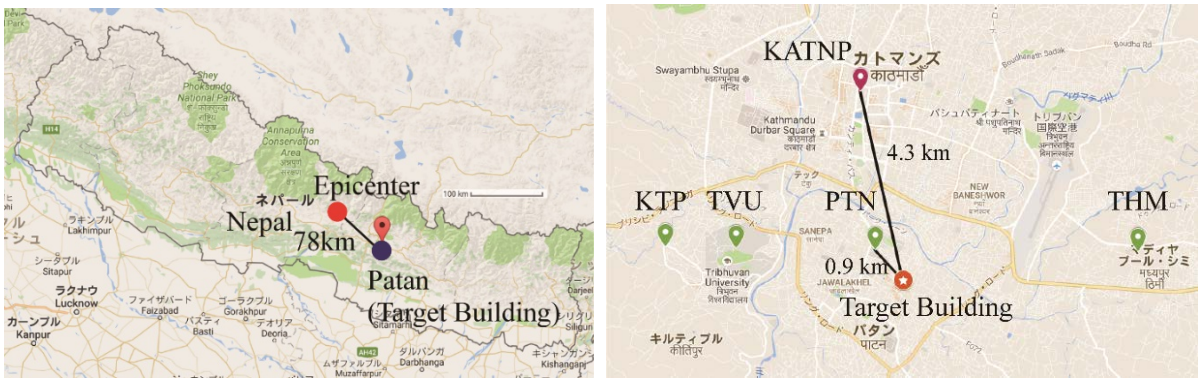

(a) Locations of the epicenter and the target building (b) Locations of the target building and the observation sites

Fig. 4 Locations of the epicenter, observation sites and target building (Google maps[13])

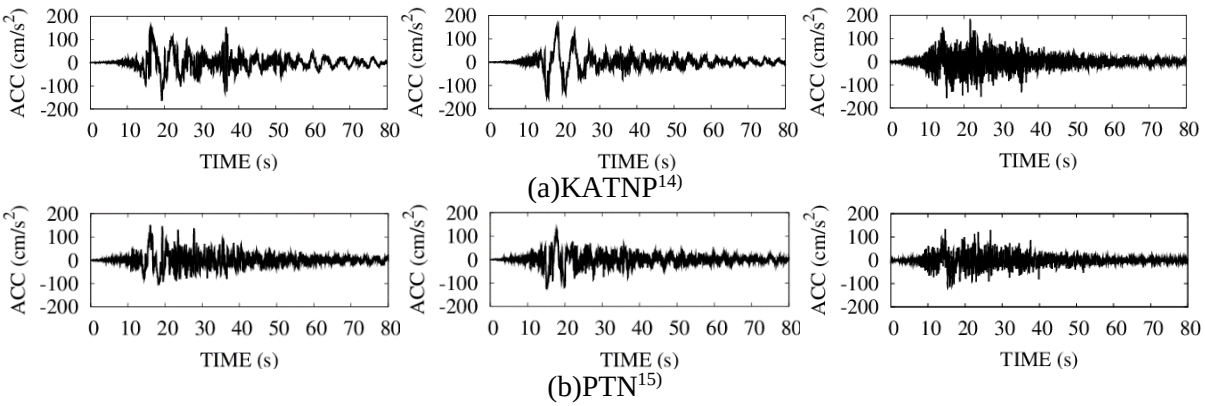

(a)KATNP[14)]

(b)PTN[15)]

Fig. 5 Acceleration record of Gorkha earthquake at KATNP and PTN（NS，EW，UD components from the left）

Table 1 Comparison of natural frequencies of the target building before and after Gorkha earthquake

Mode number (dominant direction)	Before earthquake (Hz)	After earthquake (Hz)	Change ratio (%)
1st mode (Y-direction)	4.33	4.02	−7.16
2nd mode (Both X- and Y-directions)	5.78	5.58	−3.46
3rd mode (X-direction)	6.87	6.43	−6.40
4rd mode (Y-direction)	7.13	6.68	−6.31
5rd mode (Y-direction)	8.40	7.64	−9.05

Figure 5 shows the accelerogram observed at KATNP and PTN. The peak ground accelerations at KATNP for the NS, EW and UD components were 162 cm/s^2, 155 cm/s^2 and 184 cm/s^2, respectively. The peak ground accelerations at PTN for the NS, EW and UD components were 151 cm/s^2, 128 cm/s^2 and 133 cm/s^2, respectively.

2.3 Natural frequencies of the target building before and after Gorkha earthquake

Structural damage causes a reduction in stiffness, which can be detected as a reduction in the natural frequency. Microtremor observations of the target building was conducted before the earthquake in November of 2009 and after the earthquake in March of 2016. A comparison of the natural frequency evaluated by the microtremor observations showed that the natural frequency of the target building was reduced as shown in Table 1 before and after the earthquake[11)]. X is the longitudinal direction (north-south direction) and Y is the tangential direction (east-west direction). Three acceleration records observed by three accelerometers were transformed into Fourier spectra, and natural frequencies were estimated by reading the frequencies at which the Fourier spectra takes peak values. Since the natural frequencies are reduced after the earthquake, damage that caused a reduction in the stiffness was considered to have occurred to the target building.

3. DEVELOPMENT OF NUMERICAL MODEL OF TARGET BUILDING

3.1 General remarks

In this study, a numerical model of the target building in the pre-earthquake condition was developed by refined DEM[16)]. In this chapter, the basic concept of the refined DEM, how the numerical model was established, and the verification result of the numerical model is described.

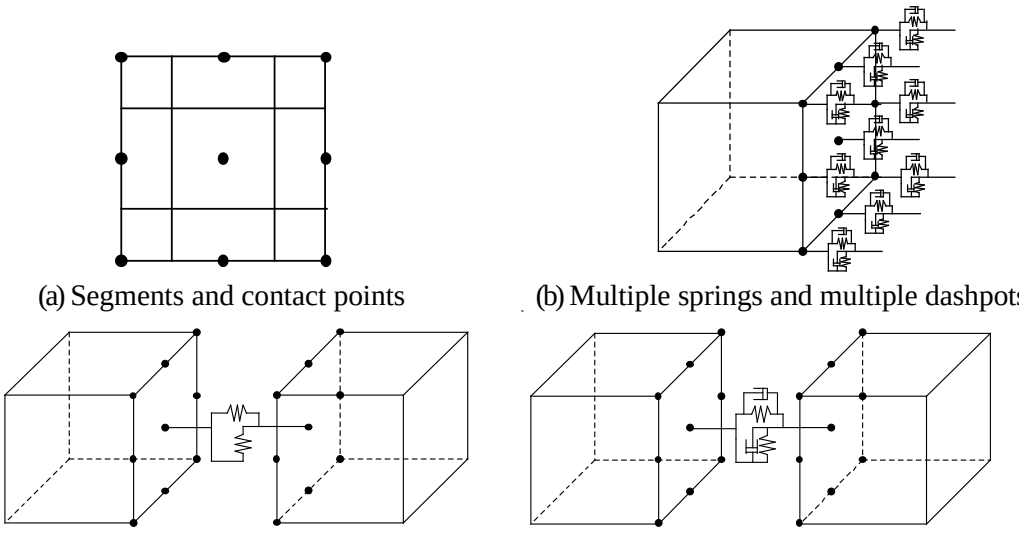

(a) Segments and contact points (b) Multiple springs and multiple dashpots

(c) Restoring spring (d) Contact spring and dashpot

Fig. 6 Refined DEM

3.2 Refined DEM

The refined DEM is a numerical analysis method for discontinuum in which the structure is modeled as an assembly of rigid elements. The original DEM[17] has the drawback that the spring constant could not be determined theoretically. The refined DEM overcame this drawback, and it discretizes the surface of the elements into segments (Fig. 6(a)) and attaches the spring and dashpots to the representative point of each segment (Fig. 6(b)). This segmentation enables the spring constant to be derived theoretically based on the equilibrium of the forces of each segment. Figure 6(c) shows a spring for computing the restoring force (restoring spring), which models the elasticity of elements. The restoring spring is set between continuous elements. Structural failure is modeled as the breakage of the restoring spring, at which time the restoring spring is replaced with a contact spring and a contact dashpot. Figure 6(d) shows the spring and dashpot for computing the contact force (contact spring and dashpot) and modeling the contact, separation, and recontact between elements. The dashpots are introduced to express energy dissipation due to the contact. For more details of the refined DEM, please refer to 16).

3.3 Modeling of the target building

3.3.1 Overview

The numerical model is shown in Fig. 7. The longitudinal direction (south-north direction) is denoted by the X-direction (The positive X-direction is the south.), and the transverse direction (east-west direction) is denoted by the Y-direction (The positive Y-direction is the east.). The width of the building is 16.5 m in the longitudinal direction and 5.6 m in the transverse direction. The height of the 1st and 2nd floors is 2.4 m and 2.2 m, respectively. The maximum height is 6.5 m.

In the numerical model that we generated prior to Gorkha earthquake[10], the roof plate, the ceiling beam and the roof truss of the second floor, the stairs, the two thin walls on the first floor, and the floor of the second story were not modeled considering that the effects of those components are negligible. However, since cracks were found in the thin wall on the first floor during the visual inspection after the earthquake, we considered it necessary to model the thin walls. In this paper, the ceiling beam and the roof truss of the second floor, the stairs, the two thin walls on the first floor and the floor of the second story were also modeled and only the roof plate was not modeled. Introducing new components into the numerical model made it possible to express the natural frequencies of multiple modes, which were observed by microtremor observation.

3.3.2 Overall view

An overall view of the numerical model seen from the south-west and north-east side is shown in Fig. 7(a)(b). A total of about 24,000 elements is used. The outside wall and inner wall is 60 cm thick. The size of the bricks used in the model is 20 cm (in-plane direction of the wall) × 10 cm (height direction) × 30 cm (out-of-plane direction of the wall). The mortar is 3 mm thick. From the visual inspection, the actual size of the bricks is about 20 cm (in-plane direction of the wall) × 5 cm (height direction), and the actual thickness of the mortar is about 3 mm.

Figure 7(c) indicates the brick elements extracted from the whole model. Figure 7(d) indicates the timber elements extracted from the whole model. Brown, gray and light purple were used to represent the brick elements. Blue, orange, green and red were used to represent the timber elements. The interface between the brick and timber elements was modeled to be bonded with mortar. As for the boundary conditions, all elements at the bottom of the numerical model were fixed.

3.3.3 Roof

The modeling of the roof is shown in Fig. 7(e). The ceiling beam and the roof truss of the second floor were modeled and the thin tin roof plate was not modeled. The model of the roof consists of timber elements. The orange horizontal ceiling beam is located between the top of the western wall and the top of the inner wall of the second floor. The blue horizontal ceiling beam is located between the top of the inner wall and the top of the eastern wall. The roof truss is composed of three vertical columns. In the actual building, the number of ceiling beams in the western and eastern sides is not the same, and the interval of the ceiling beam is not constant. But for simplicity, we assumed that the number of ceiling beams in the western and eastern sides is the same and the interval of the ceiling beams is set to be constant. The width of the columns and the beams is 20 cm in the model, which is the average size of the actual columns and beams.

3.3.4 Stairs

Figure 7(f) shows a model of the stairs. In our previous study[10], the stair was not modeled, and there was a large free space near the southern wall. The stairs are made of timber. The green elements show the stairs, and the blue elements show the plate set beneath the stairs, and the red elements show the beams between the stairs and the plate.

3.3.5 Outside wall

The southern wall is shown in Fig. 7(g). The entrance of the building is located in the southern wall and the western wall has larger openings compared to the northern wall. The brown elements indicate bricks. The frames of the doors and windows are composed of timber with a width of 20 cm. The vertical timbers are shown in green and the horizontal timbers above and beneath the openings are shown in red.

The western wall is shown in Fig. 7(h). The western wall faces the main road and has the largest openings. Only the window frames were modeled. In the small windows on both sides of the first floor, small perforated pieces of wood are inset for ventilation, and there is an unperforated piece of wood (blue).

The eastern wall is shown in Fig. 7(i). The eastern wall has five windows on each floor, and only wooden window frames were modeled. Compared to the western wall, the eastern wall has fewer openings, but it also has fewer timbers.

The northern wall is shown in Fig. 7(i). It has only two windows on the second floor and only the timber window frames were modeled. Compared to the southern wall, the northern wall has fewer openings, but it also has fewer timbers.

3.3.6 Inner wall

The inner wall is shown in Fig. 7(k)(l). The building has an inner wall that runs in the south-north direction on both floors. On the inner wall on the first floor, the doors allow access between the eastern and western rooms. In the north-east corner of the first floor, there is a thin wall connecting the inner wall and the eastern wall (brick elements of light blue), and there is a small room in the north-east corner,

which is used as a warehouse. The thin wall was modeled as 20 cm thick. Cracks have been identified at both ends of this thin wall (D1 and D2 in Fig. 2(a)). In the north-west side of the first floor, there is a thin wall connecting the inner wall and the western wall, and the thin wall was modeled as 20 cm thick (The thin wall is modeled with pink brick elements and the door frame is modeled with green and red timber elements.). A crack (D3 in Fig. 2(a)) is observed at the joints between the thin wall (light purple) and the inner wall (gray) as described before. As described later, the gray and yellowish green elements are color-coded to represent the crack of D3 generated at the boundary between the gray and yellowish green elements.

3.3.7 Floor

The floor of the second story seen from above is shown in Fig. 7(m). The first-floor ceiling seen from the bottom is shown in Fig. 7(n). In past research[10], the floor consisted of timber members placed horizontally in the east-west direction. Therefore, the floor of the second story is basically full of gaps, which may have made the horizontal rigidity very low. In this study, the floor of the second story was constructed by placing a 10-cm high brick (grey, light purple) on a 20-cm high wooden beam (orange, green, blue). During the damage survey, many cracks were found in the floor on the south side. It is thought that this is because the opening is large on the south side and it is much more easily shaken than the north side. In the numerical model, the place where the crack could not be confirmed was colored in gray, and the part where a lot of cracks were found was colored in light purple.

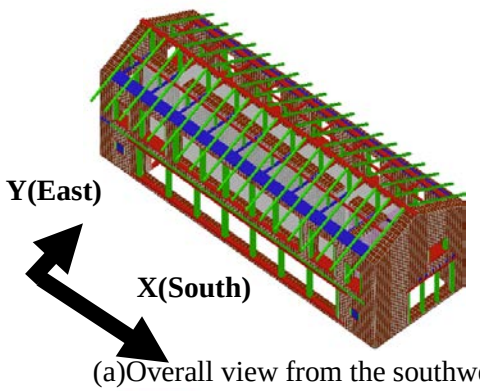

(a)Overall view from the southwest

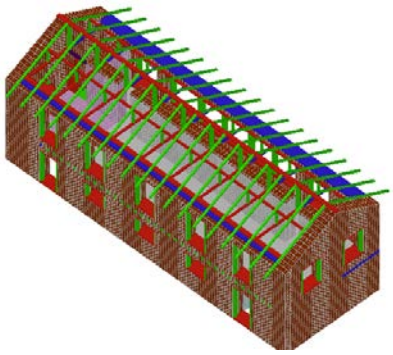

(b) Overall view from the northeast

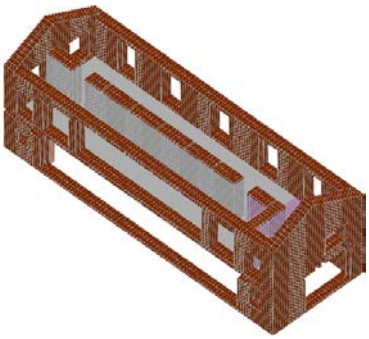

(c)Figure of bricks seen only from the southwest

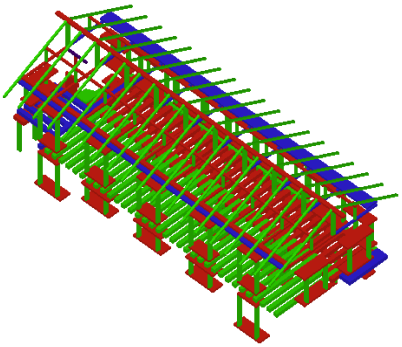

(d)Figure of timbers seen only from the northeast

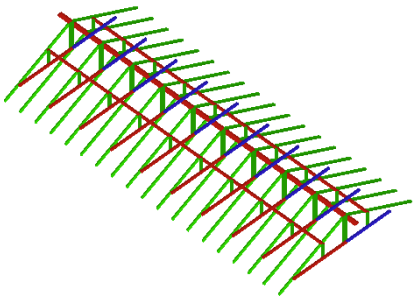

(e)Roof truss seen from the southwest

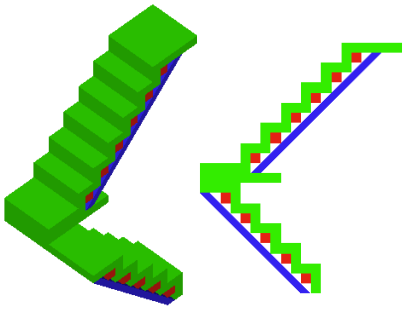

(f)Stairs seen from the southwest and the south

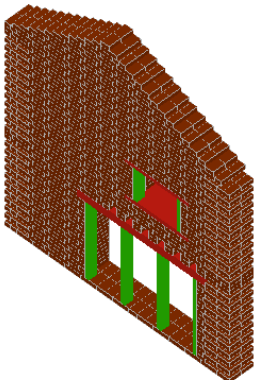

(g)Southern wall seen from the southeast

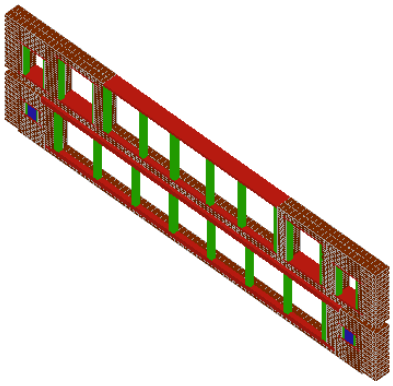

(h)Western wall seen from the southwest

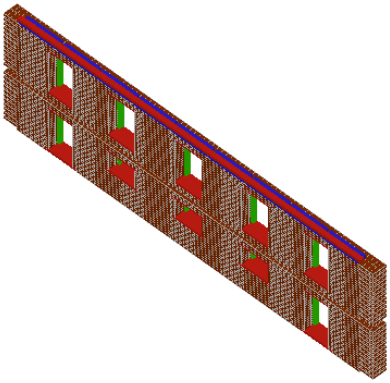

(i)Eastern wall seen from the southeast

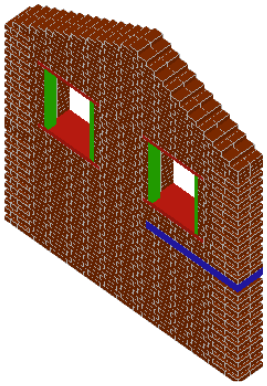

(j)Northern wall seen from the northwest

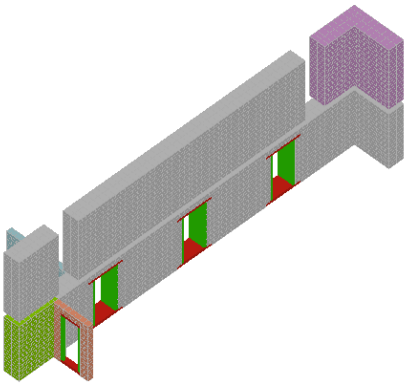

(k)Inner wall seen from the northwest

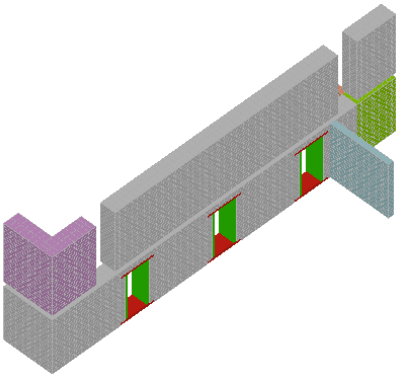

(l)Inner wall seen from the southeast

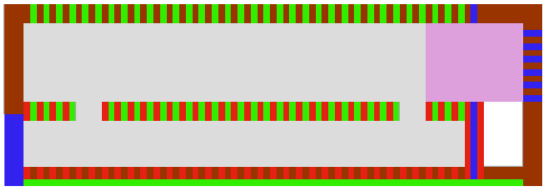

(m)2nd floor from above (Right is south.)

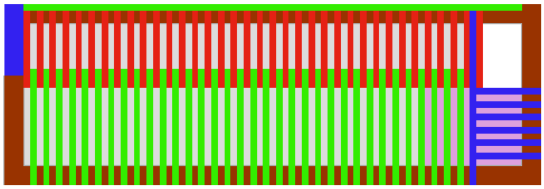

(n)1st floor ceiling from the bottom (Right is south.)

Fig. 7 Numerical model

Table 2 Material properties

	Brick of outer wall	Brick of inner wall	Mortar for outer wall	Mortar for inner wall	Timber
Density(t/m^3)	1.768	1.768	1.768	1.768	0.800
Young's modulus (MPa)	470	600	470	600	1250
Poisson's ratio	0.11	0.11	0.25	0.25	0.12

Table 3 Comparison of natural frequencies of microtremor observation and analysis

Microtremor observation before earthquake		Analysis results (Hz)		Error (%)
Mode order (Dominant direction)	Dominant frequency (Hz)	Mode order (Dominant direction)	Dominant frequency (Hz)	
1st (Y-direction)	4.33	1st (Y-direction)	4.20	−3.10
2nd (X- and Y-directions)	5.78	2nd (X- and Y-directions)	6.25	7.52
3rd (X-direction)	6.87	3rd (X-direction)	6.93	1.01
4th (Y-direction)	7.13	4th (Y-direction)	7.71	7.52
5th (Y-direction)	8.40	5th (Y-direction)	8.90	5.62

3.4 Material properties

The material property values used for the analysis are shown in Table 2. The material property values of bricks and mortar were used with reference to the values of the experimental results of the masonry in Nepal, which was conducted in previous research[10].

The average Young's modulus of masonry composed of brick and mortar was used as the Young's modulus of each of the bricks and mortar. Since the Young's modulus of the masonry body estimated from the experiment varied from 274 to 632 MPa, the value that reproduces the natural frequency obtained by the microtremor observation was found by trial and error within this range.

Regarding the material properties, the values of timbers, the mass, stiffness and Poisson's ratio used in the past study related to the target area were used[18].

The dashpots placed between the contact elements (Fig. 6 (d)) are considered to be viscous damping, and a critical damping of 1.0 (a damping constant of 100%) was given to efficiently dissipate energy from collisions in the same manner as that in previous studies[10].

3.5 Validation of numerical model

A square wave with an amplitude of 100 gal (1 gal = 1 cm/s^2) and a duration of 0.01 s was input to the analysis model as ground acceleration, and free vibration was caused. Response displacements were output at various points on the model. It was assumed that mortar does not break and gravity was not considered. The natural frequency and mode shape were calculated from the Fourier spectrum of the displacement response in each of the X- and Y-directions when rectangular waves were separately input in the X- and Y-directions.

Table 3 compares the natural frequencies of the first to fifth modes obtained by microtremor measurement before the earthquake and numerical analysis. The mode shape is shown in Fig. 8. It has been confirmed that the natural frequencies from the first to fifth order can be roughly reproduced, and that the dominant direction matches the actual direction. From the above, we considered the constructed analysis model valid.

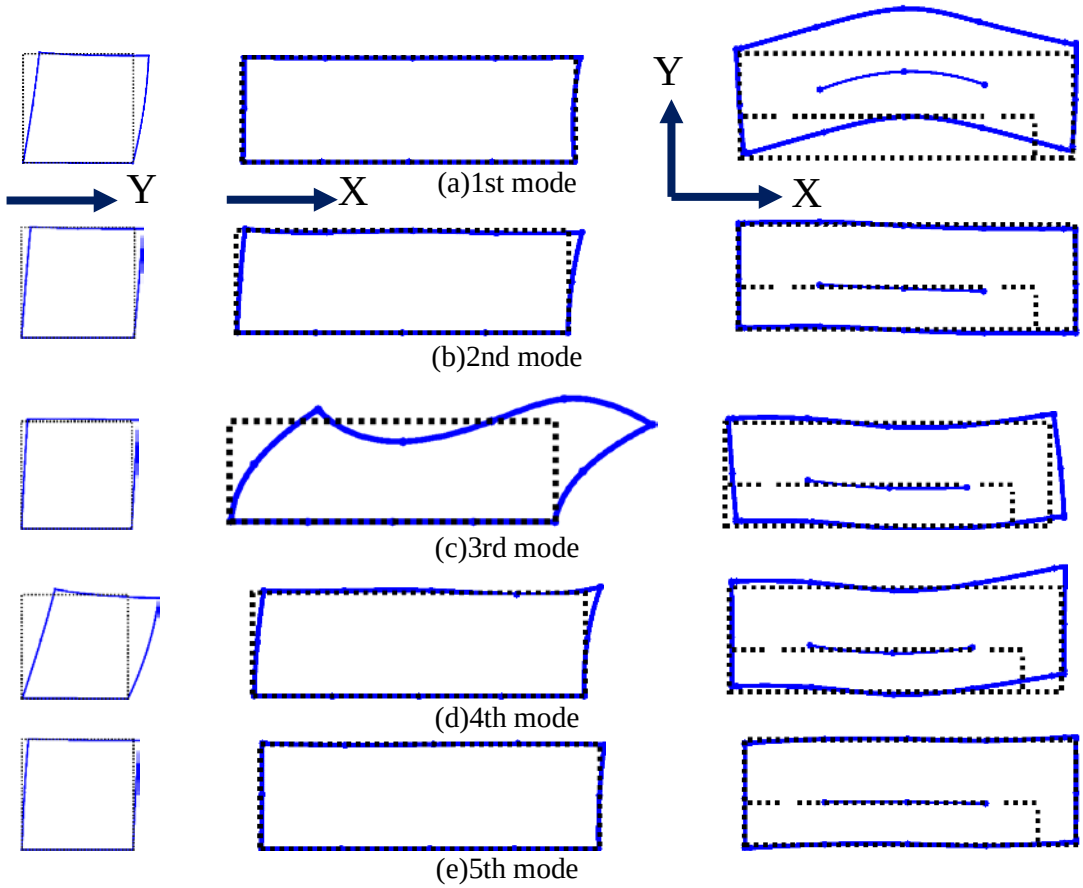

Fig. 8 Mode shape (Left: South wall seen from the front, Middle: West wall seen from the front, Right: Second floor seen from above)

4. ESTIMATION OF GROUND MOTION AT TARGET BUILDING SITE

4.1 Microtremor observation

The microtremors were measured in November of 2016 at three locations: the road in front of the target building, strong motion station KATNP approximately 4.2 km away from the target building, and strong motion station PTN approximately 0.9 km away from the target building. As KATNP was installed in the US Embassy and we could not enter the building, it was measured at the parking lot of the next building. Since PTN seismographs are installed on the first floor in the Tribhuvan University building, they were measured on the road in front of the building. It took measurements for 12 minutes using three microtremor observation devices JU-410 of Hakusan Corporation. JU-410 has a resolution of 24 bits for AD conversion. The built-in sensor is a servo-type accelerometer. The measurement range was ±0.2 G, ±2 G, and ±4 G, and ±0.2 G were selected. The array radius was 1.73 m for the target building and PTN, and 1 m for KATNP.

4.2 Microtremor observation results

The H/V spectral ratio is shown in Fig. 9 (a). The ratio of the power spectrum was taken to make it easy to see the difference between each site. The H/V spectral ratio shows that all three units show comparable results, revealing little difference between machines. From the results of the H/V spectral ratio, it is considered that the deep ground structure was very similar because the primary natural frequency of the ground was around 0.4 Hz at all three sites. However, at the target building site, a peak was seen around 3 Hz to 8 Hz, but not at either KATNP or PTN sites.

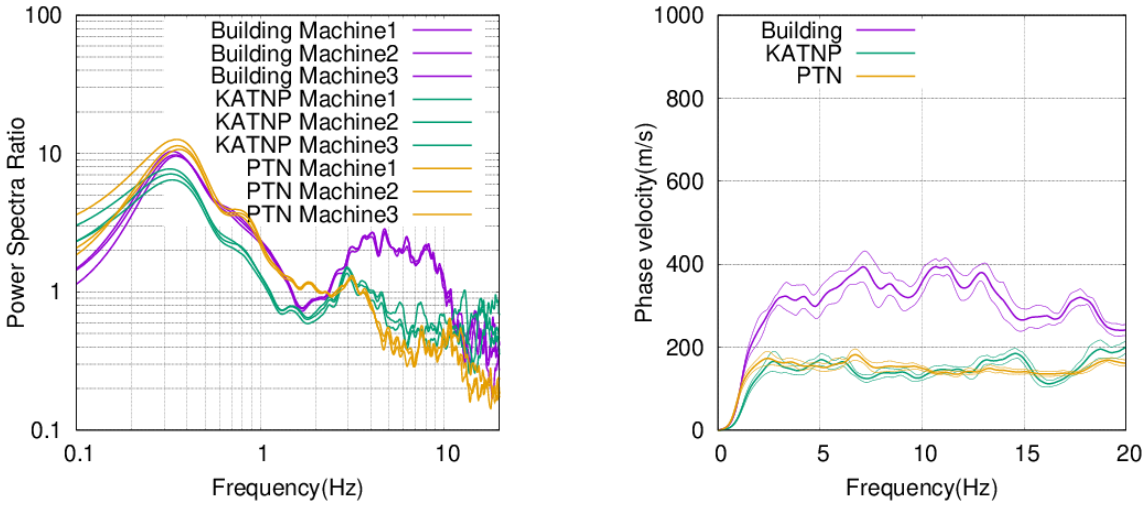

(a) H/V spectral ratio (ratio of power spectra) (b) Rayleigh wave phase dispersion curve

Fig. 9 Microtremor observation results

Next, Fig. 9 (b) shows a comparison of the phase dispersion curves of Rayleigh waves. The phase dispersion curves of KATNP and PTN look similar, but that of the target building site looks different from those of the other two sites. In general, the phase velocity of the dispersion curve asymptotically approaches the shear wave velocity of the surface ground at high frequencies. Therefore, it can be inferred that the surface ground profile is different between the building location and those of the other two sites. Also, since the natural frequency of the target building before the earthquake was 4.33 Hz for the first mode, 5.78 Hz for the second mode, and 6.87 Hz for the third mode, it is possible that the frequency components important for the target building were included more in the ground motion at the building site than those at KATNP and PTN.

In addition, it was reported that the shear wave velocity of the surface ground was about 150 m/s from the result of past surface wave exploration in PTN[19]. In Fig. 9(b), the phase velocity of the Rayleigh wave asymptotically approaches 150 m/s on the high frequency side, which indicates that the result is consistent with that of previous research.

From the above, we decided to estimate the earthquake ground motion at the target building site. It may be desirable to estimate the ground motion by temporary aftershock observations. However, temporary aftershock observations were not performed. Moreover, array observations could not be performed with a large radius, so the underground structure profiles could not be estimated. Therefore, we decided to use an empirical ground motion estimation method using the H/V spectral ratio.

4.3 Ground motion estimation using the H/V spectra ratio

There are several methods[20), 21), 22)] of estimating the earthquake ground motion at unobserved points using only the microtremor H/V spectral ratio and the earthquake ground motion record observed at nearby strong motion stations. In this method, modification factors β_O and β_E are defined as follows:

$$\beta_O = \frac{1/C_{Omax}(H/V)_O^M}{(H/V)_O^E}, \quad \beta_E = \frac{1/C_{Emax}(H/V)_E^M}{(H/V)_E^E}. \tag{1}$$

Here, subscripts *O* and *E* indicate the observation point and estimation point, respectively; superscripts *M* and *E* indicate the microtremors and earthquake, respectively; and C_{Omax} and C_{Emax} are the maximum amplitudes of the microtremor H/V spectral ratios at the observation and estimation points, respectively. In summary, modification factors β_O and β_E were obtained by dividing the normalized microtremor H/V spectral ratios by the H/V spectral ratios of the earthquake ground motion.

By introducing modification factors β_O and β_E, the microtremor H/V spectral ratio at the observation and estimation sites can be obtained as follows:

Table 4 Comparison of estimation error (the root mean square)

Estimation method	The case when ground motion at PTN is estimated from ground motion records at KATNP		The case when ground motion at KATNP is estimated from ground motion records at PTN		Sum of the root mean square
	NS direction	EW direction	NS direction	EW direction	
Maruyama et al.	0.87	0.68	0.84	0.99	3.38
Harada et al.	0.72	0.70	0.81	0.74	2.97
Nakamura et al.	0.71	0.75	0.82	0.73	3.01

$$\frac{(H/V)_E^M}{(H/V)_O^M} = \frac{C_{Emax}\beta_E(H/V)_E^E}{C_{Omax}\beta_O(H/V)_O^E}. \quad (2)$$

From the above equation, the horizontal Fourier earthquake amplitudes at estimation site H_E^E were obtained using the earthquake's horizontal Fourier amplitudes at observation site H_O^E and modification factor α, as follows:

$$H_E^E = \alpha \frac{(H/V)_E^M}{(H/V)_O^M} H_O^E. \quad (3)$$

The case where the modification factor α of equation (3) is 1 is the proposed equation by Maruyama et al.[20] In the proposed method by Harada et al.[21] and Nakamura et al.[22], modification factor α can be estimated as follows:

$$\alpha = \frac{\beta_O}{\beta_E} \cdot \gamma_{E/O} \cdot \frac{1/C_{Emax}}{1/C_{Omax}}, \quad \gamma_{E/O} = \frac{{V_E}^E}{{V_O}^E}. \quad (4)$$

In the above equation, to estimate modification factor α, all parameters except modification factor β_E and the spectral ratio of vertical ground motions $\gamma_{E/O}$ can be computed from the H/V spectral ratios. However, modification factor β_E and the spectral ratios of vertical ground motions $\gamma_{E/O}$ cannot be obtained without the earthquake ground motion records at the estimation site. Empirical equations for estimating these unknown parameters have been proposed by Harada et al.[21] and Nakamura et al.[22]. Details are given in Refs. 21) and 22).

4.4 Verification of ground motion estimation method using the H/V spectra ratio

We applied estimation methods to the Kathmandu Valley. Specifically, the acceleration waveform of PTN was estimated using the acceleration waveform of KATNP and the H/V spectrum ratio at two sites of KATNP and PTN. On the contrary, the acceleration waveform of KATNP was estimated using the acceleration waveform of PTN and the H/V spectrum ratio of two sites. The estimation error was evaluated by the root mean square of the estimation error of the acceleration Fourier amplitude. The estimation error is shown in Table 4.

Although the difference between the estimation errors by Harada et al. and Nakamura et al.'s methods is small, we decided to adopt Harada et al.'s method because the error of Harada et al.'s method is slightly smaller. As an example, Fig. 10 shows a comparison of the observation waveform of KATNP, the observation waveform of PTN and the estimated waveform of PTN from the recording of KATNP by the method of Harada et al.

4.5 Estimation of ground motion at the building site using the H/V spectra ratio

In this study, we used Harada et al.'s method. Harada et al.'s method only estimates the amplitude of the Fourier spectrum of the ground motion at the estimation site, but the phase of the Fourier spectrum

is also necessary to calculate the ground motion at the estimation site. Harada et al.'s method uses the phase of the Fourier spectrum of the observed ground motion at nearby strong motion stations as that of the ground motion at the estimation site. In this study, we also used the phase of the observed ground motion. Figure 11 shows the acceleration Fourier amplitude and acceleration history of the target building site estimated based on the observation records of KATNP. Since this method can be used to estimate the horizontal component, we used the KATNP's vertical ground motion record as the input vertical ground motion for the building.

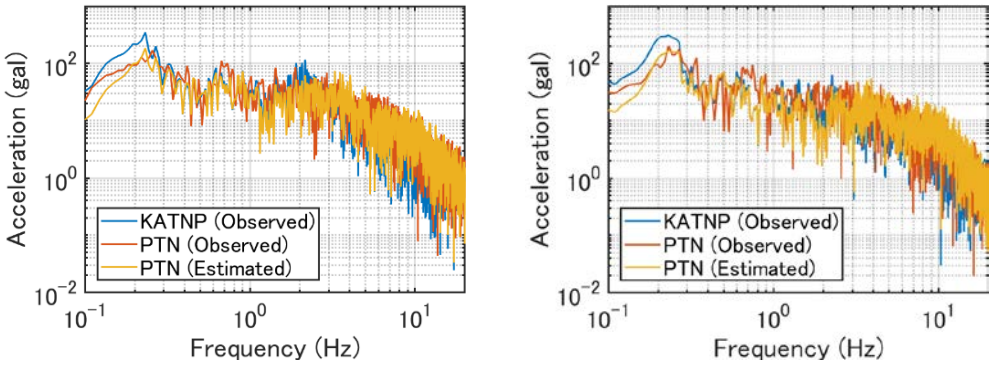

(a)NS component (b)EW component

Fig. 10 Comparison of amplitude of acceleration Fourier spectra among observed record at KATNP (blue), observed record at PTN (red) and estimation of PTN record by Harada et al.'s method (yellow)

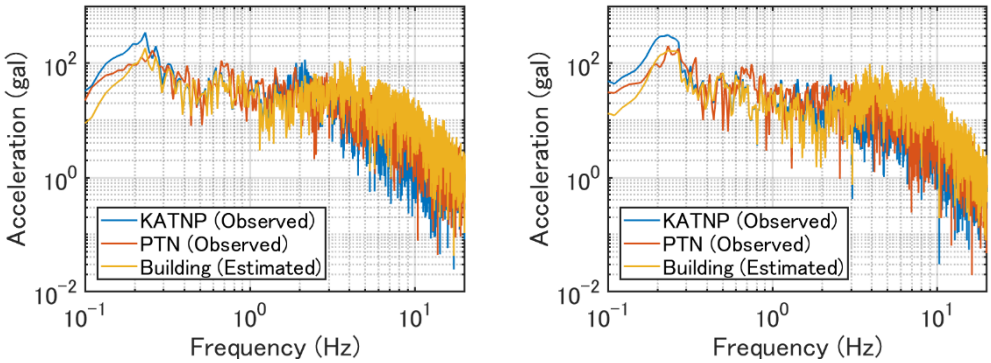

(a) amplitude of acceleration Fourier spectra (blue: KATNP observed record, red: PTN observed record, yellow: Estimation for the building site)

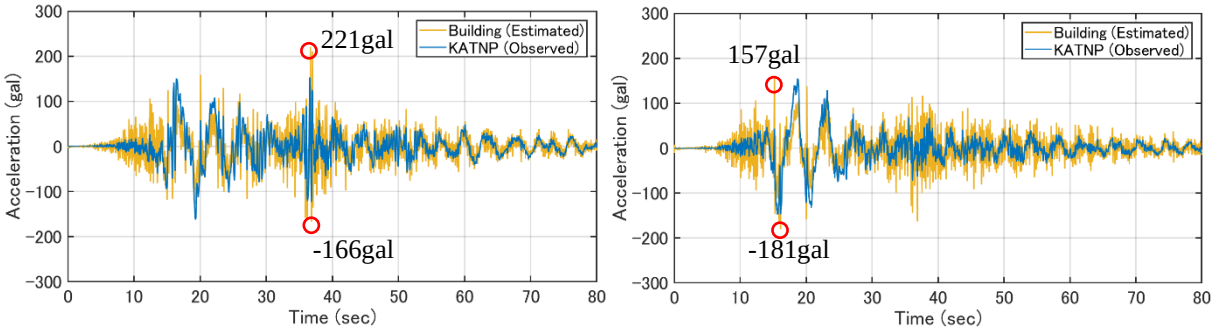

(b) acceleration history (blue: KATNP observed record, yellow: Estimation for the building site (the data from 10 to 40 s was used for the analysis)

Fig. 11 Estimated ground motion at the building site (left: NS component, right: EW component)

Table 5 Mortar strength

Tensile strength (MPa)	Bond strength (MPa)	Friction angle (°)	Compressive strength (MPa)
0.1	0.0917	42.5	1.58

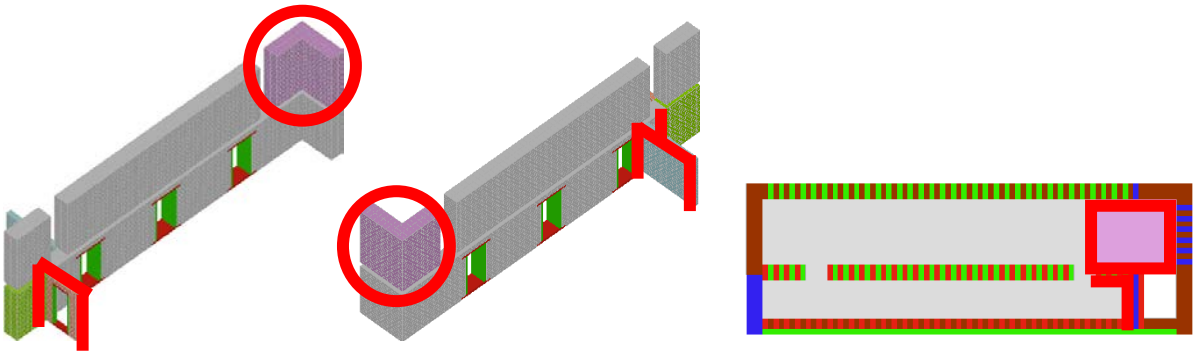

(a)Inner wall from the northwest (b)Inner wall from the southeast (c)2nd floor from above (The right is the south.)

Fig. 12 The areas where failure occurrence is allowed for Analysis Model B (the area indicated by a thick red line and the area surrounded by thick red circles and a square)

5. SEISMIC RESPONSE ANALYSIS

5.1 Outline

In this chapter, the estimated ground motion calculated in Chapter 4 is input to the analysis model of the building before the Gorkha earthquake constructed in Chapter 3. The natural frequencies of the building after the Gorkha earthquake are calculated by Fourier transformation of the displacement response of the building after the Gorkha earthquake input.

5.2 Analysis outline

5.2.1 Input ground motion

The duration of the input ground motion was 38 s. For the first 30 s (0 to 30 s), we input the estimated ground motion from 10 s to 40 s, which have a large amplitude (Fig. 11). For the next 3 s (30 to 33 s), an acceleration of 0 gal was given to cause free vibration, and the response was attenuated. For the subsequent 0.01 s (33 to 33.01 s), a constant acceleration of 100 gal was input, and for about 5 s (33.01 to 38 s), the acceleration was given 0 gal again for free vibration. The natural frequencies after the earthquake were determined by the Fourier transform of the response displacement during the last 5 s of free vibration.

5.2.2 Material property and strength

The values shown in Table 2 were used for the density, Young's modulus and Poisson's ratio. The damping constant of the dashpot was set to critical damping 1.0 (damping constant 100%).

As for the strength between elements, it was assumed that failure only occurred in mortar between bricks, and timber was not destroyed. The strength of the mortar is shown in Table 5. The compressive strength, bond strength and friction angle of the mortar obtained by experiments in past researches[15] was used. As experimental values were not obtained for the tensile strength of mortar, 0.1 MPa was assumed with reference to the Indian design standard[18] used in Nepal.

Here, two analysis models were created according to the difference in the area where mortar failure is considered.

Analysis Model A is a model that assumes that failure occurs in all mortars.

Analysis Model B is a model that assumes tensile failure, shear failure (bond strength, friction angle) and compressive failure to the mortar only where cracks are actually confirmed by visual inspection after an earthquake. The mortar where the crack was not confirmed is modeled not to break. The areas considered for failure are shown in Fig. 12,

- Both ends and the upper end of the first-floor pink inner wall shown in Fig. 12 (a) (both ends (shown by the green circle ●) and the upper end of the pink wall in Fig. 2)

- Both ends and the upper end of the first-floor light blue inner wall shown in Fig. 12 (b) (D1 and D2 (shown by the red circle ●) and the upper end of the light blue wall in Fig. 2)
- The joint part between the yellow-green wall and the gray wall shown in Fig. 12 (b) (D3 shown by the red circle ● in Fig. 2)
- The inner wall of the second floor shown in pink in Fig. 12(a)(b)(c) and the second-floor near the stairs (D4, D5, D6 shown by the red circle ● in Fig. 2)

Assuming that minor cracks and window frame cracks have little effect on stiffness reduction, no failure of those part was considered.

5.3 Analysis results

5.3.1 Analysis Model A

Figure 13 shows the cracking situation at the time when the estimated ground motion of Gorkha earthquake for 30 s was input to Analysis Model A. The outline of the element is shown in blue, and the location where the tensile failure occurs is indicated by the red line. In the narrow wall on the south side, diagonal cracks can be seen mainly on the second floor. In the longitudinal wall on the east side, diagonal cracks are observed mainly on the second floor, and horizontal cracks can be confirmed at the bottom of the first and second floor walls. From the occurrence of cracks, it can be inferred that the deformation in the Y-direction is outstanding.

Next, the natural frequencies after the earthquake were obtained from the Fourier transform of the displacement response from 33 s to 38 s. Table 6 shows a comparison of the natural frequencies before and after the earthquake between the microtremor and the analysis model. In the numerical analysis after the earthquake, only one outstanding mode in the X- and Y-directions was obtained, so only the comparison between the first mode (first mode in the Y-direction) and the third mode (first mode in the X-direction) is shown. In Analysis Model A, the first-mode natural frequencies in the X- and Y-directions after the earthquake are significantly lower than those before the earthquake and are much lower than those obtained by microtremor measurement after the earthquake. This also corresponds to the fact that the area of tensile failure that occurred in Analysis Model A was wider than the crack occurrence area confirmed by visual inspection on site, and the result of Analysis Model A was an overestimation of the actual damage. From the above, it is considered that the tensile strength of the actual buildings may be larger than the 0.1 MPa assumed in this study.

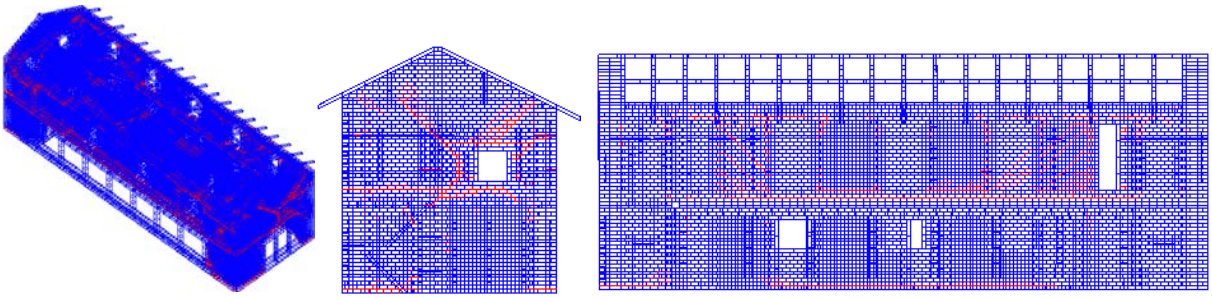

(a) View from the southwest (b) View from the south (c) View from the east

Fig. 13 Failure occurrence after 30 s of ground motion input (Analysis Model A)

Table 6 Comparison of natural frequency before and after the earthquake (Hz)

Mode order (Dominant direction)	Before earthquake		After earthquake		
	Microtremor observation	Analysis Models A, B	Microtremor observation	Analysis Models A	Analysis Model B
1st (Y-direction)	4.33	4.2	4.02	3.2	4.0
3rd (X-direction)	6.87	6.93	6.43	5.8	6.7

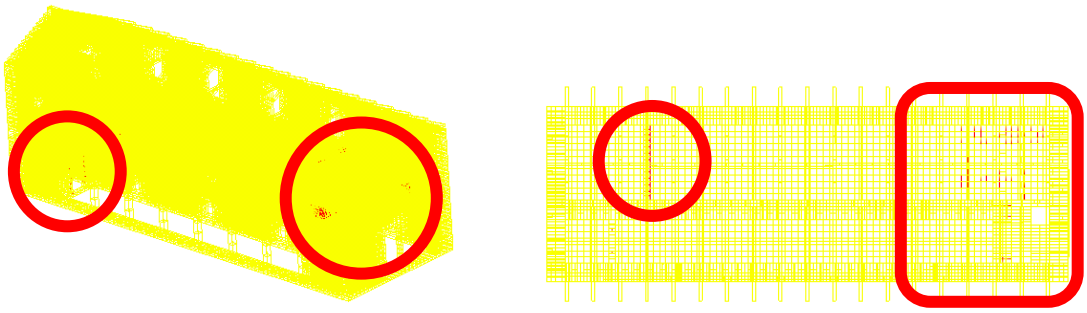

(a) View from southwest (b)View from above (The right is the south.)

Fig. 14 Failure situation after 30 s of ground motion input (Analysis Model B)

5.3.2 Analysis Model B

In Analysis Model B, the failure was only allowed to occur at the locations where cracks were confirmed by visual inspection. Figure 14 shows the cracking situation when the estimated ground motion of Gorkha earthquake with a duration of 30 s was input to Analysis Model B. The outline of the element is shown in yellow, and the location where tensile failure occurred is indicated by the red line. Although it is difficult to discriminate from Fig. 14, it was confirmed that a tensile failure occurred at the locations where damage occurrence is allowed as shown in Fig. 12, and the failure occurred as expected.

Next, the natural frequencies after the earthquake were obtained from the Fourier transform of the displacement response from 33 to 38 s. Table 6 compares the natural frequencies before the earthquake (microtremor, analysis model) and the natural frequencies after the earthquake (microtremor, Analysis Model A, Analysis Model B). The first-mode natural frequency after the earthquake of Analysis Model B was very close to the actual value obtained by microtremor measurement. In Analysis Model B, the third natural frequency after the earthquake actually decreased by 0.44 Hz from 6.87 Hz to 6.43 Hz, whereas in the analysis, it decreased by 0.23 Hz from 6.93 Hz to 6.7 Hz. Analysis Model B underestimated the reduction in the natural frequency, but the analytical natural frequency of Analysis Model B was closer to the actual natural frequency after the earthquake compared to that of Analysis Model A.

Based on the above, it was confirmed that the first-mode natural frequency after the earthquake can be roughly reproduced by assuming damage to the thin walls shown with D1 to D6 and the green circle in Fig. 2 where the damage was found or suspected by visual inspection.

6. CONCLUSIONS

This study investigated the causes of natural frequency reduction due to Gorkha earthquake in a two-story masonry building with high historical value located in Patan district of Nepal. In the field survey, microtremors were observed at the target building site and KATNP and PTN, which are strong motion observation stations. From the H/V spectral ratio and the phase dispersion curve of the Rayleigh wave, it was found that the surface ground profiles at the target building site and the strong motion observation sites were different. Therefore, the ground motion at the target building site was estimated from the H/V spectrum ratio and the ground motion record using the empirical method proposed by Harada et al.

In addition, since the natural frequencies of the building were measured before and after the earthquake in the target building, an analysis model that can reproduce the natural frequencies and its dominant direction from the 1st to 5th modes before the earthquake was developed based on the refined distinct element method.

The estimated ground motion was input to the created analysis model, and seismic response analysis of the target building was performed. When the tensile strength was set with reference to the Indian design standards used in Nepal, failure was judged to have occurred over a wider area than the actual area, and the natural frequencies decreased significantly in the analysis compared to the actual values observed after the earthquakes. From the above, it was found that the tensile strength of the actual

building may be larger than the tensile strength according to the Indian design standards.

When we use an analysis model that allowed the occurrence of failure only in places where cracks were confirmed by visual inspection after the earthquake, the decrease in the first-mode natural frequency due to the earthquake was reproduced with good accuracy. In other words, the decrease in the first-mode natural frequency could be explained by the cracks that were confirmed by visual inspection, so damage that affected the decrease in the first-mode natural frequency of the building could be found by visual inspection.

Using the method described in this paper, by measuring the natural frequencies of a masonry structure before and after an earthquake it is possible to examine the damage location that caused the decrease in the natural frequencies. The same numerical analysis procedure can be used for masonry damage prediction.

ACKNOWLEDGMENT

This research used the outcome of the Global COE Program for Education, Research and Development of Strategy of Ritsumeikan University ("Disaster Mitigation of Cultural Heritage and Historic Cities") conducted before Gorkha earthquake. The authors are very grateful to the late Prof. Hitoshi Taniguchi for his kind encouragement and warm support during our research.

REFERENCES

1) Bilham, R. and Ambraseys, N.: Apparent Himalayan slip deficit from the summation of seismic moments for Himalayan earthquakes 1500-2000, *Current Science*, Vol. 88, No. 10, pp. 1658–1663, 2005.
2) Disaster Preparedness Network Nepal: Earthquake, http://www.dpnet.org.np/index.php?pageName=earthquake (last accessed on February 28, 2018)
3) Rohit K. R.: *Heritage homeowner's preservation handbook*, UNESCO, 2007.
4) UNDP: Seismic hazard mapping and risk assessment for Nepal, *Report submitted to the Ministry of Housing and Physical Planning*. UNDP/UNCHS (Habitat), NEP/88/054/21.03, 1994.
5) Yoshida, M. and Upreti, B.N.: Central Himalayan earthquake and Kathmandu crisis, *Chigakukyoiku and Kagaku-undo*, Vol. 53, pp. 41–51, 2006. (in Japanese)
6) Upreti, B.N. and Yoshida, M.: Seismic hazard and mitigation activities in Nepal with emphasis on Kathmandu Valley, *Journal of South Asian Studies*, Vol. 2, No. 11, pp. 1–16, 2009.
7) Sakai, H: Stratigraphic division and sedimentary facies of the Kathmandu Basin Group, central Nepal, *Journal of Nepal Geological Society*, Vol. 25, pp. 19–32, 2001.
8) Sakai, H.: Tectonics of the 2015 Nepal earthquake and extremely soft ground in Kathmandu, *Japan Geological Society News*, Vol. 18, No. 5, pp. 9–10, 2015.
9) JICA: *Final Report on Kathmandu Valley Earthquake Disaster Mitigation Plan for Nepal*, 2002.
10) Research Center for Disaster Mitigation of Urban Cultural Heritage, Ritsumeikan University and Institute of Engineering, Tribhuvan University: *Disaster Risk Management for the Historic City of Patan, Nepal, Final Report of the Kathmandu Research Project*, 2012.
11) Furukawa, A., Kiyono, J., Parajuli, R.R., Parajuli, H. R. and Toki, K.: Evaluation of damage to an historic masonry building in Nepal through comparison of dynamic characteristics before and after the 2015 Gorkha Earthquake, *Frontier in Built Environment*, Vol. 3, Article 62, 2017. doi: 10.3389/fbuil.2017.00062.
12) Bureau of Indian Standards: National Building Code of India, http://bis.org.in/sf/nbc.htm, 2016. (last accessed on February 28, 2018)
13) Google Maps: https://www.google.co.jp/maps?hl=ja (last accessed on February 28, 2018)
14) Combined Strong-Motion Data (CESMD): Earthquakes Recorded by Station KATNP, http://www.strongmotioncenter.org/cgi-bin/CESMD/StaEvent.pl?stacode=NPKATNP (last

accessed on February 28, 2018）
15) Takai, N., Shigefuji, M., Rajaure, S., Bijukchhen, S., Ichiyanagi, M., Dhital, M. R. and Sasatani, T.: Strong ground motion in the Kathmandu Valley during the 2015 Gorkha, Nepal earthquake, *Earth Planets Space*, Vol. 68, Article 10, 2016.
16) Furukawa, A., Kiyono, J. and Toki, K.: Proposal of a numerical simulation method for elastic, failure and collapse behaviors of structures and its application to seismic response analysis of masonry walls, *Journal of Disaster Research*, Vol. 6, No. 1, pp. 51–68, 2011.
17) Cundall, P.A. and Strack, O.D.L.: A discrete numerical model for granular assemblies, *Geotechnique*, Vol. 29, pp. 47–65, 1979.
18) Jaishi, B., Ren, W., Zong, Z.H. and Maskey, P.N.: Dynamic and seismic performance of old multi-tiered temples in Nepal, Engineering Structures, Vol. 25, pp. 1827–1839, 2003.
19) Sawada, K., Takai, N., Yadab, D., Shigefuji, M., Okajima, H., Miyahara, Y. and Sasatani, T.: Estimation of Strong Ground Motion at Kathmandu basin: Study on surface ground conditions of strong motion stations and earthquake record, *Proceedings of the 2013 Annual Conference of the Architectural Institute of Japan*, pp. 239–240, 2013. (in Japanese)
20) Maruyama, Y., Yamazaki, F., Motomura, H. and Hamada, T.: Estimation of strong motion distribution using the H/V spectrum ratio of microtremor, *Journal of Japan Society of Civil Engineers*, No. 675/I-55, pp. 261–272, 2001. (in Japanese)
21) Harada, T., Nakamura, M., Wang, H. and Saitoh, S.: A Method of Estimation of Earthquake Ground Motion Using Nearby Records and Microtremors H/V Spectral Ratio, *Journal of Applied Mechanics*, Vol. 11, pp. 595–602, 2008. (in Japanese)
22) Nakamura, M., Harada, T., Wang, H. and Saitoh, S.: A method of estimating earthquake ground motion using microtremor H/V spectral ratio, *Journal of Japan Society of Civil Engineers* (*Structural Engineering & Earthquake Engineering* (*SE*/*EE*)), Ser. A1, Vol. 65, No. 1 (*JSCE Journal of Earthquake Engineering*, Vol. 30), pp. 65–74, 2009. (in Japanese)

(Original Japanese Paper Published: May 2019)
(English Version Submitted: August 28, 2019)
(English Version Accepted: September 10, 2019)